ACS Catalysis

pubs.acs.org/acscatalysis

Correspondence/Rebuttal

CO Methanation over Ni−Fe Alloy Catalysts: An Inverse Design Problem

Wenqiang Yang, Zhenbin Wang, and Jens K. Nørskov*

Cite This: ACS Catal. 2024, 14, 11657−11665

Read Online

ACCESS | Metrics & More | Article Recommendations | Supporting Information

ABSTRACT: We propose an approach to solve the inverse design problem in heterogeneous catalysis in which the goal is to find a material composition and structure that will maximize the active surface site under reaction conditions with knowledge of the active site motif being given. Taking CO methanation over Ni−Fe bimetallic alloys as our basis catalyst systems, we aim to identify a Ni−Fe bulk/surface composition that can provide the highest activity under reaction conditions. First, the stability of various (211) surfaces with different surface and bulk compositions is studied, especially if the CO adsorption could induce surface segregation has been well studied since CO is found to dominantly cover the surface during CO methanation. Due to a similar binding strength of CO over Ni and Fe, we did not observe surface segregation induced by CO adsorption. Reaction kinetics on the corresponding stable surfaces are obtained through coverage- and surface-consistent MKM. The 4-Fe $Ni_3Fe(211)$ surface site, which corresponds to 4 Fe atoms on the surface, is the most active site among all the stable surfaces. This high activity is attributed to the presence of a pure Ni step site and an adjacent Fe site, which are particularly active for CO activation (CO + H → COH) and dissociation (COH → C + OH), respectively. Additional calculations on reaction barriers for these two rate-controlling steps on similar $Ni_3Fe(211)$ surfaces confirmed that the 1-Fe $Ni_3Fe(211)$ surface, despite being less stable, shows lower reaction barriers, suggesting the potential for further activity enhancement. Consequently, we propose that optimizing $Ni_{1-x}Fe_x$ catalysts for CO methanation may involve synthesizing Ni_3Fe catalysts with a focus on stabilizing the active site motif identified under the reaction conditions. The proposed approach offers a strategic pathway for researchers aiming to solve the inverse design problem for catalysts in other reaction systems.

INTRODUCTION

In recent years, with the increasing development of supercomputers, computational heterogeneous catalysis, especially density functional theory (DFT) aided studies, have become increasingly able to point toward "active sites" on the surface of a material that provides optimal catalytic activity and/or selectivity for a given chemical or electrochemical reaction. Given knowledge of the optimal active site, the question becomes, which bulk composition, particle size, and support will provide surfaces with a high concentration of the active site motif under the reaction conditions? This is the "inverse design problem" first defined by Zunger et al.[1−4] in their work to find the optimal atomic configuration of a complex, multicomponent system having a target electronic (bandgap) property. Very few studies have been done on the inverse design problem in heterogeneous catalysis despite a large number of studies reporting the identification of active sites for various reaction systems.[5−38] We attempt here to take on the challenge of devising theoretical methods to facilitate the inverse design problem in heterogeneous catalysis. Solving the "inverse design problem" relies on an understanding of materials' processes and how they are determined dynamically by the reaction conditions. While progress has been made on the equilibrium structure of nanoparticles, little is understood about the nonequilibrium kinetics that govern catalyst surface structure during actual catalytic processes. To solve the inverse design problem in heterogeneous catalysis will involve three tracks: (i) development of models for adsorption-induced segregation to the surface as a function of bulk composition and particle size under reaction conditions, (ii) development of reaction kinetics as a function of surface composition for selected reactions, and (iii) combination of kinetics and surface segregation/restructuring.

The prerequisite to solving the "inverse design problem" for a reaction system is a comprehensive understanding of the catalysts and the active site motif under reaction conditions. We choose here the CO methanation as our model reaction system since the reaction mechanisms and catalysts of which have been well studied since it was first proposed by Sabatier and Senderens in1902. CO methanation has been widely used in various industrial processes such as removal of trace amounts of CO from H_2-rich feed gas[39] or purification of the reformate gas for NH_3 synthesis and processes in relation to Fischer−Tropsch synthesis.[40,41] Recently, there is a rising interest in producing synthetic natural gas via the CO methanation process.[41,42] Besides, selective methanation of CO in H_2-rich gas mixtures has also attracted attention as a technique to selectively remove CO from the hydrogen-rich gas before feeding to fuel cells.[43,44] CO hydrogenation over

Received: April 25, 2024
Revised: July 4, 2024
Accepted: July 5, 2024

https://doi.org/10.1021/acscatal.4c02449
ACS Catal. 2024, 14, 11657−11665

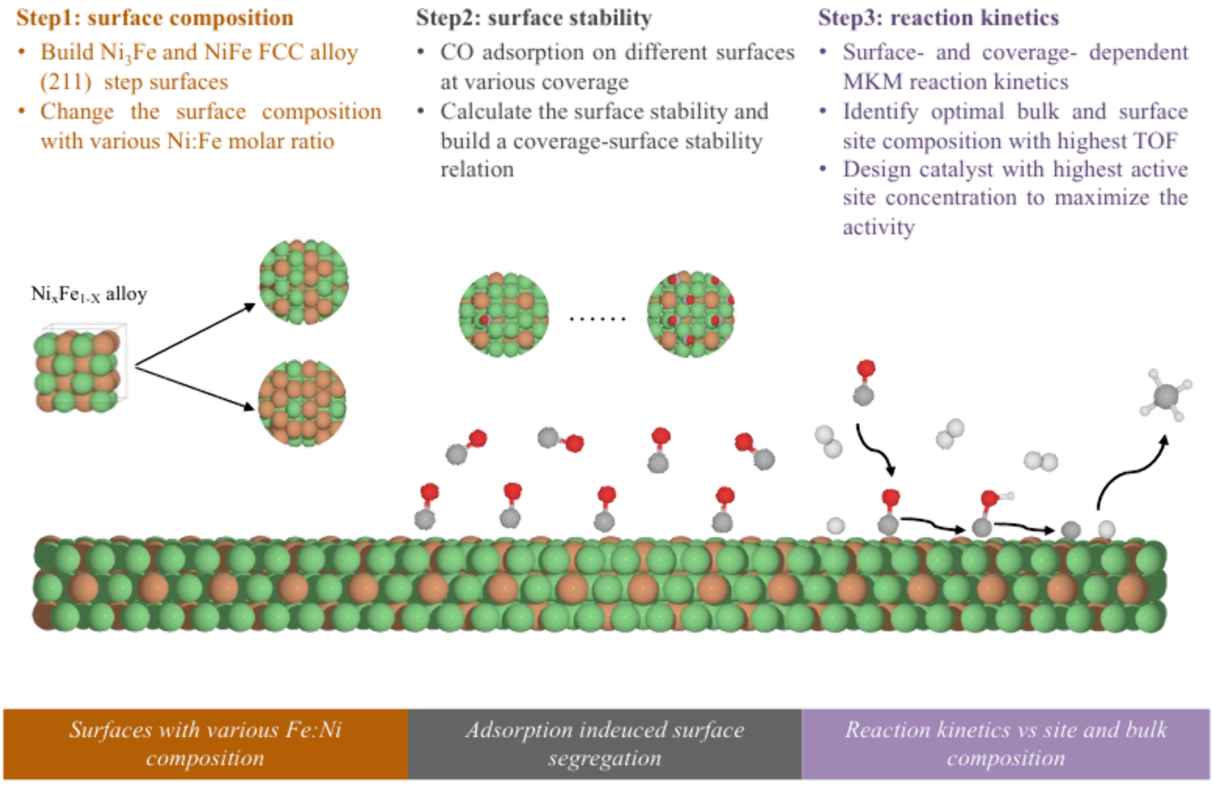

Figure 1. Proposed approach to solve the inverse design problem for the CO methanation process over Fe−Ni alloy catalyst. The brown, green, red, white, and gray balls represent Ni, Fe, O, H, and C, respectively, which applies for all the following figures.

various supported metal catalysts[19,26,39,45−49] has been investigated from the viewpoint of synthesizing CH_4. Among all the studied catalyst systems, Ni-, Ru- and Rh-based catalysts proved to be very active in selectively producing methane.[26,45,49] Especially, many studies have focused on Ni-based catalysts due to their comparatively strong methanation capabilities and low cost.[48,50] It has been suggested that bimetallic catalysts can be more active than their corresponding monometallic ones in CO hydrogenation reactions, such as Fe−Co,[51] Co−Ni,[41,52] and Ni−Fe[53−55] alloys. Especially for CO methanation reactions, Ni−Fe alloys have been widely studied as they appear to not only have higher activity but also increased selectivity toward CH_4 formation compared to the pure Fe- and Ni-based catalysts.[53,54,56,57]

We therefore take Ni−Fe bimetallic alloys as our basis catalyst systems for the CO methanation catalyst inverse design problem. We aim to build the correlation between the catalytic activity and the alloy bulk/surface site composition under the reaction conditions to find the optimal catalyst compositions to maximize the active site concentration. Herein, we propose to take three steps: Step 1) Figure out how the equilibrium surface composition changes as a function of surface coverage and the bulk composition. Especially, will surface segregation happen with the covering of dominant surface intermediates on the surface? We will specifically study the effect of CO adsorption on the stability of surfaces for different Ni_xFe_{1-x} bulk alloys. We assume CO dissociation is the rate-limiting step and the surface will mainly be covered by CO.[58,59] We are trying to find the most stable surface composition (surface Fe/Ni ratio) at various CO coverages. Step 2) Identify surface site composition with the optimal rate/activity, which needs to get the reaction rate on various surfaces that is stable under different CO coverages. We propose here a self-consistent surface- and coverage-dependent microkinetic model (MKM) to solve the reaction kinetics, which is fully described in the methods section. And, finally, step 3) correlate the surface stability and reaction kinetics to guide the catalyst design with maximum active site/activity. The workflow of our approach is well displayed in Figure 1, and the details of each step are well described in the following methods section. To this end, we endeavor not only to provide a comprehensive approach for the inverse design of heterogeneous catalysts that is not limited to the study of CO methanation but also to provide researchers with a protocol for the catalyst synthesis of other well-studied reactions.

COMPUTATIONAL MODELS AND METHODS

Surface System Model. To study the stability of the surface upon CO adsorption and find out if it would induce surface metal segregation under reaction conditions, surfaces with various compositions have been built and CO adsorption at different coverages has been studied. We manipulate the surface Fe:Ni molar ratio to get surfaces with various surface Fe/Ni compositions and it is conducted by increasing/decreasing the number of surface Ni atoms by replacing them one by one with Fe atoms until the surface is fully covered by Ni or Fe. Unlike the traditional surface model, which only consists of a single surface slab, we build here a surface system model that consists of one surface slab and one corresponding bulk, which is denoted as surface-bulk in the following sections to differentiate it from the $Ni_{1-x}Fe_x$ bulk alloy. In each step of the surface slab Ni to Fe atom exchanging process, there is a corresponding Fe to Ni atom exchanging process in the surface-bulk, which manifests the beauty of the proposed surface system model that the Ni:Fe composition of

https://doi.org/10.1021/acscatal.4c02449
ACS Catal. 2024, 14, 11657−11665

the bulk alloy will be preserved for its all corresponding surface systems. This will enable us to correctly correlate the surface activity to the bulk alloy composition, which is also closer to the real surface under reaction conditions. The formation energies of replacing one and two bulk Fe atoms by Ni atoms of various sizes for the surface-bulk have been calculated and are shown in Figure S1. For all the studied models, there is no significant difference found in the formation energy, a 4 × 4 × 4 bulk is therefore used as the surface-bulk to balance the size effect and the cost of computational resource. For the surface-slab, a 6 × 4 × 3 slab being separated by a 15 Å vacuum is used. A representative surface system model is shown in Figure 2a, and a detailed description of the atom exchanging process can be found in section S1.

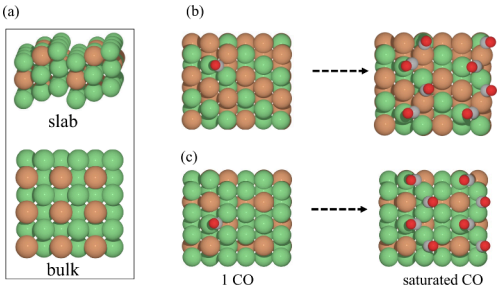

Figure 2. (a) Representative surface system model used in this work, and the optimized stable 1 CO and saturated/8 CO covered (b) 12-Fe surface-slab and (c) 4-Fe surface-slab for NiFe and Ni_3Fe surface systems, respectively.

Computational Methods. All the calculations were carried out using the Vienna Ab Initio Simulation Package (VASP) based on density functional theory (DFT) with the projector augmented wave (PAW) method.[60−63] The generalized gradient approximation[62,64] (GGA) with the RPBE[65] functional was used to treat exchange−correlation effects. An energy cutoff of 400 eV is used for all DFT calculations, and the energy convergence criterion was set to 10^{-5} eV. All structures were relaxed until the Hellmann−Feynman force on each atom were smaller than 0.03 eV $Å^{-1}$. FCC Ni, Ni_3Fe and NiFe and BCC Fe are used for the bulk alloy corresponding to a bulk molar percentage of Fe of 0%, 25%, 75% and 100%, respectively. For all the surface slab calculations, the top half slab atoms are fully relaxed in all directions during optimizations, while the half underneath are fixed. To obtain the vibration entropy of the surface adsorbates, the adsorbate vibrational frequency calculations have been conducted with all metal atoms being fixed at their optimized positions. All the calculations are spin polarized, and a dipole correction is applied to the direction perpendicular to the surface slab. The ferromagnetic state was considered for both Ni and Fe atoms in this work.[66] The Brillouin zone integration was sampled by a 2 × 2 × 1 k-points mesh for the surface using the Monkhorst−Pack scheme.[67] To search for the transition state (TS) of each elementary reaction step involved in the CO methanation, a combination of the climbing image nudged elastic band[68] (CI-NEB) method and the dimer[69,70] method was used to precisely locate the TS.

Surface- and Coverage-Dependent MKM. To understand the reaction kinetics of the CO methanation over the Fe−Ni alloy catalyst, the kinetic model should consider the surface coverages and build on the corresponding stable surfaces under reaction conditions. We thus propose here a self-consistent surface- and coverage-dependent MKM framework to obtain the reaction kinetics (activity) under the reaction conditions. First, in step 1) an initial coverage for CO $\theta_{CO,i}$ is set, and the free energies of adsorbates and transition states (TSs) on the corresponding stable surface under the specific CO coverage are calculated. By parametrizing the MKM with the calculated free energies, a new coverage $\theta_{CO,n}$ will be obtained. In step 2) the convergence check will be conducted to check if the criteria are satisfied: the new CO coverage $\theta_{CO,n}$ agrees with the initial CO coverage $\theta_{CO,i}$ (the difference is smaller than 0.05, which is the coverage difference of adsorbing one more CO on the surface), and the used surface is the most stable one under the resulting new CO coverage. If either of the two criteria is satisfied, then in step 3) recalculate the free energies of adsorbates and TSs on the new surface that is stable at the new CO coverage $\theta_{CO,n}$ and update the MKM with the recalculated free energies which again will give another updated new CO coverage. Step 2 will be conducted again to check whether the convergence criteria are satisfied. The convergence checking and recalculating processes will be repeated until the two criteria in step 2 are satisfied. A workflow of the proposed self-consistent MKM is presented in Figure 3. We note that a similar self-consistent

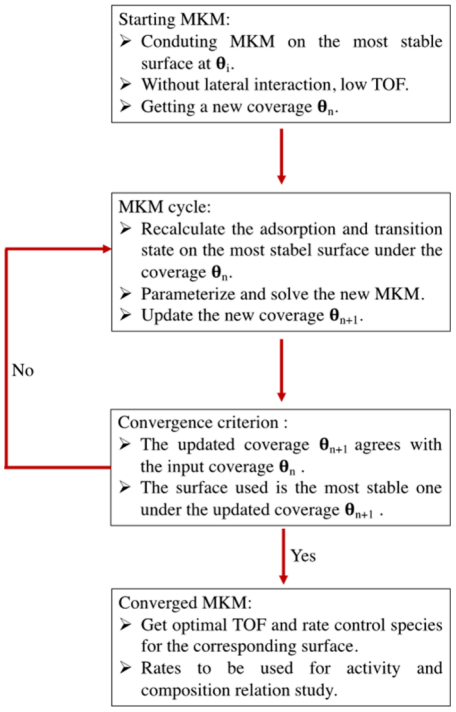

Figure 3. Workflow of the self-consistent surface- and coverage-dependent microkinetic model.

MKM was previously proposed by Guo et al.,[71] which considered coverage consistency. In addition to surface coverage, we also considered surface composition consistency by recalculating the reaction energies (transition states and adsorption) on the surface that is stable at the MKM output CO coverages. This ensures that the surface used in the MKM is always the most stable at the MKM CO coverages. For the MKM building, a mean field model with lateral interaction is used to simulate the CO methanation process. The steady state reaction kinetics are obtained by solving the microkinetic

https://doi.org/10.1021/acscatal.4c02449
ACS Catal. 2024, 14, 11657−11665

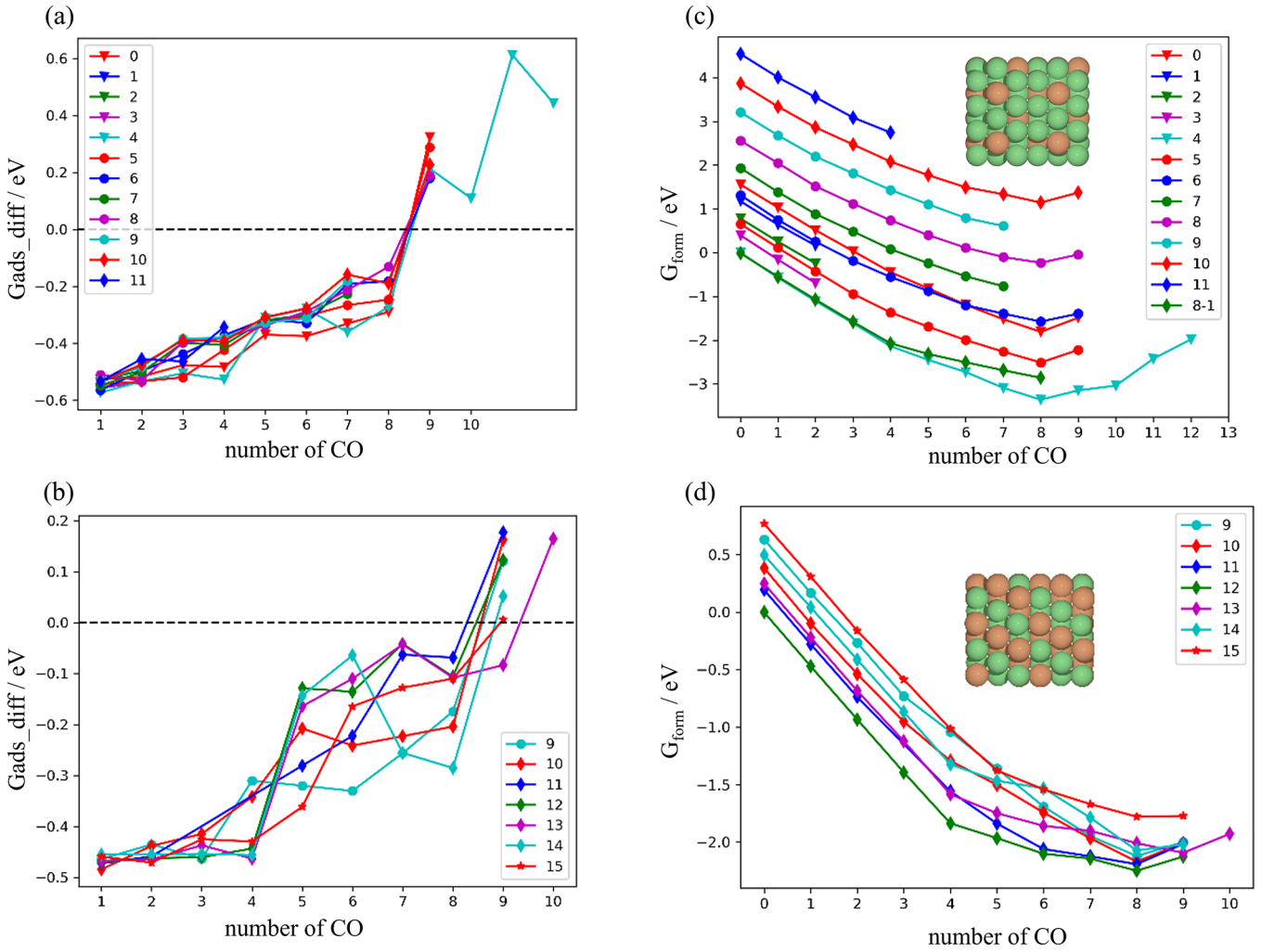

Figure 4. Differential adsorption energy of CO on various (a) $FeNi_3(211)$ surfaces and (b) FeNi(211) surfaces. The relative formation energies of various (c) $FeNi_3(211)$ and (d) FeNi(211) surface systems. The number in the figure legend represents the number of Fe atoms on the surface. The free energy is calculated at a temperature of 523 K and a partial pressure of 1 and 0.02 bar, respectively, for H_2 and CO. The inset figures in (c) and (d) are the most stable surfaces for Ni_3Fe and NiFe which contain 4 and 12 surface Fe atoms, respectively.

model via the ODE solver ode15s implemented in MATLAB with no assumptions regarding to the rate controlling steps.

RESULTS AND DISCUSSION

Does CO Adsorption Induce Surface Segregation? To study whether CO adsorption could induce surface segregation is equivalent to studying the stability of surfaces of various surface Fe/Ni molecular ratios upon CO adsorption. The first task is thus to build surface systems consisting of a surface slab with different Fe/Ni compositions. For the Ni_3Fe and NiFe alloys studied in this work, there exists natural surface slabs that follow an atom stacking pattern originating from its stable bulk. For the Ni_3Fe alloy, there are two natural surface slabs that contain 4 and 8 Fe atoms on the surface, respectively, while only one natural surface slab is found for the NiFe alloy that consists of 12 surface Fe atoms. For all the surface system, a $6 \times 4 \times 3$ surface slab is used, indicating a total of 24 atoms on the outmost surface slab layer. With the corresponding natural surface slabs as the starting point, we conducted the replacing process as described in section S1 to step by step increase/decrease the surface Fe concentration of the surface slab. To clearly differentiate the surface systems, it is named the number of surface Fe atoms. For instance, 4-Fe $Ni_3Fe(211)$ is the surface system of $Ni_3Fe(211)$ and consists of 4 surface Fe atoms and correspondingly 20 surface Ni atoms since the total surface atoms is 24. All possible surface slab configurations have been considered for each of the replacing steps and the resulting optimized most stable surface slab at each step for $Ni_3Fe(211)$ and NiFe(211) surface systems are shown in Figure S4 and Figure S5, respectively. Generally, the Fe atoms are symmetrically distributed without surface aggregation on both the $Ni_3Fe(211)$ and NiFe(211) surfaces. This indicates that Fe clustering on the surface is unlikely, as it would require Fe atom diffusion on the surface, which our calculations show to be thermodynamically unfavorable. Therefore, Fe clustering on the surface is not considered in the current work. The next task is to study the stability of these surface systems upon CO adsorption under the reaction conditions. To get the stability of the surface systems, we calculated the relative surface formation free energy, referring to the corresponding clean natural surface systems. The details of the calculation of the relative surface formation free energy are explained in section S4. For CO adsorption calculations, all possible sites, including the ontop, bridge, 4-fold hollow, hcp, and fcc hollow sites, have been considered. It should be noted that in the calculations, not only the position of the sites but

https://doi.org/10.1021/acscatal.4c02449
ACS Catal. 2024, 14, 11657−11665

also the composition of the sites (Ni/Fe ratio) have been considered so that the most stable CO adsorption is always obtained. The site definition and a full list of the sites are described in section S5 in the Supporting Information. CO adsorption at various surface coverages is calculated by gradually increasing the surface coverage from 0 ML to θ_{sat} (the saturated CO coverage on the surface). For calculations at each coverage, all possible unoccupied adsorption sites are included to ensure that the most stable adsorption configuration is always obtained and is used for the next one CO adsorption.

For all the surface systems considered for Ni_3Fe and NiFe alloy, CO favors the hcp-hollow site at the step edge over all other sites and prefers to first adsorb on the site that has the maximum number of Ni atoms, such as the hcp-sst-NiNiNi and the hcp-sst-NiFeNi on the 4-Fe $Ni_3Fe(211)$ and 12-Fe NiFe(211) surfaces, respectively, as shown in Figure 2b,c. CO absorbs on step bridge sites after all the 3-Ni and 2-Ni hcp-hollow sites have been occupied. The optimized stable CO adsorption configuration at coverages from 0 ML to θ_{sat} on the 4-Fe $Ni_3Fe(211)$ and the 12-Fe NiFe(211) surface system are shown in Figure S7 and Figure S8, respectively. The preference of CO adsorption on Ni demonstrates an active role of Ni in CO activation, which is verified by the following reaction kinetics results. The differential binding free energies of CO at various coverages are shown in Figure 4a,b, respectively, for all the studied $Ni_3Fe(211)$ and NiFe(211) surface systems. It clearly shows that the surface is saturated with CO adsorption after taking 8 CO since the ninth CO adsorption becomes unfavorable in energy. This is because there are only 8 step sites (hcp-hollow and bridge) on the surface slab and because CO prefers the step sites over all other sites. A 1 ML CO-covered step site agrees with our assumption that the surface will be dominantly covered by CO under reaction conditions and has also been found in previous studies.[58] To investigate the stability of the surface under reaction conditions, particularly at the reaction temperature and CO pressures,[53] we calculated the relative surface formation energies (surface migration energies) using equations S1−S3 in the Supporting Information. All energies are Gibbs free energies at 523 K and are referenced to the CO gas phase at a reaction pressure of 0.02 bar, based on previous experimental studies.[54] The relative formation free energies of the studied surfaces under various CO coverages are shown in Figure 4c,d; the surface system with natural stacking surface slab is found to be the most stable system for both $Ni_3Fe(211)$ and NiFe(211) surfaces irrespective of whether the surface is partially or fully covered by CO. For the $Ni_3Fe(211)$ system, the two natural stacking surface systems, 8−1 and 4 in Figure 4c which consist of 8 and 4 surface Fe atoms, respectively, are both stable at lower CO coverage, while the 4-Fe surface system becomes more stable at higher CO coverage. Similarly, for the NiFe surface system, the natural stacking surface system (12 in Figure 4d) is always the most stable one. The as-found stability trend demonstrates that CO adsorption will not cause surface composition change and thus will not induce surface segregation on the Ni−Fe alloy surface. This is because of a very close binding free energy for CO adsorption on Ni(211) and Fe(211) surfaces, which are −0.51 and −0.41 eV, respectively, under the reaction conditions.[54] Even though CO adsorption is 0.10 eV more stable in energy on Ni(211), it is not strong enough to drive a Ni atom migration to the surface, and therefore, no surface segregation occurred upon CO adsorption. It should be noted that there should be 25 surface systems theoretically (from 0 Ni covered surface to a fully 24 Ni covered surface) each for $Ni_3Fe(211)$ and NiFe(211); however, as shown in Figure 4c,d, we found that the further the surface composition is away from the natural stacking surface, the less stable it will be. We thus studied 13 surface systems for the $Ni_3Fe(211)$ surface and even less (only 7) for the NiFe(211) surface.

Reaction Kinetics: Which Composition Gives the Optimal Activity? For the CO methanation process, we considered three possible reaction pathways, namely, the direct CO dissociation path (CO-path), the H-assisted COH path (COH-path), and CHO (CHO-path) path in which CO is hydrogenated first and followed by the dissociation of COH and CHO to C and CH,[20] respectively. The full reaction network is listed in section S6 in the Supporting Information. According to the surface stability results, the natural stacking surface system is always the most stable one under all the CO coverages, and the 4-Fe and 12-Fe surface system is therefore used for Ni_3Fe and NiFe catalyst calculations, respectively. This leads to the reduction of the surface- and coverage-dependent MKM from a two-dimensional model down to a one-dimensional model, an only coverage-dependent MKM. The free energies of all the involved intermediates and TSs are first calculated on the clean surface (input $\theta_{CO} = 0$) and used to initiate the self-consistent MKM. Recalculations and convergence checking are then conducted until the MKM convergence criteria are satisfied. The binding free energies of all of the surface intermediates and transition states at various coverages are provided in Tables S1−S4, respectively, for the 4-Fe $Ni_3Fe(211)$, 12-Fe NiFe(211), Ni(211), and Fe(211).

From the converged MKM, the surface coverages, TOFs, and dominant pathways have been obtained and are shown in Table S5 in the Supporting Information. The most important task is, however, to correlate the activity/TOF to the bulk/surface composition of the Ni−Fe alloy catalysts. which is shown in Figure 5. It can be clearly seen that the Ni−Fe alloys have larger TOFs than both the two pure metal catalysts and an optimal (largest) TOF is found on the 4-Fe $Ni_3Fe(211)$ surface system, which agrees with previous experimental and theoretical studies;[54,56,57] meanwhile, Fe(211) is found to have the lowest TOF. The trend can be explained by the dominant pathways and rate-limiting species. On the Fe(211) surface,

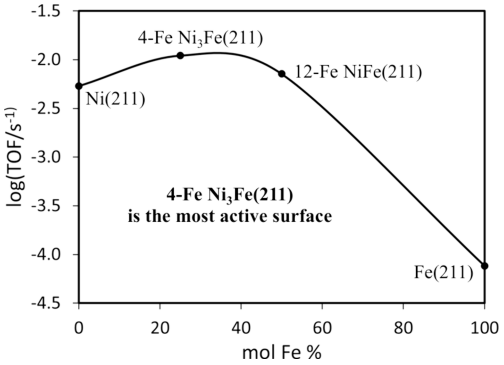

Figure 5. Optimal TOF for various surface systems studied in this work, where the TOF for each surface is the one from the most stable surface at the corresponding converged CO coverage from the self-consistent MKM. The reaction condition is set at a temperature of 523 K and a partial pressure of 1 and 0.02 bar, respectively, for H_2 and CO.

https://doi.org/10.1021/acscatal.4c02449
ACS Catal. 2024, 14, 11657−11665

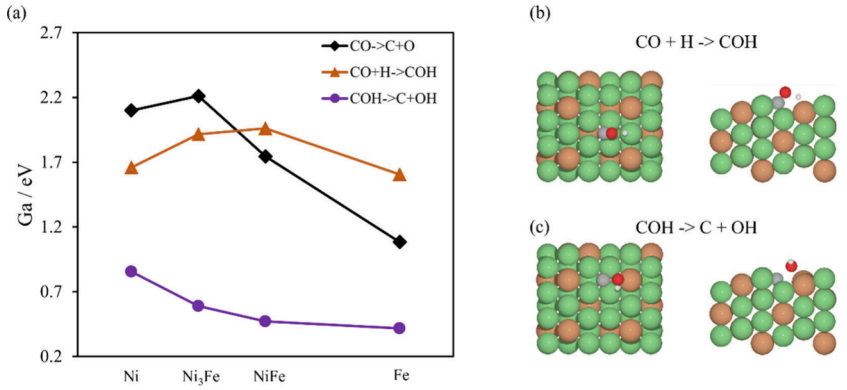

Figure 6. (a) Reaction barrier for CO dissociation, COH formation and COH dissociation on different catalyst surfaces. (b) Active site for COH formation reaction and (c) COH dissociation reaction on $Ni_3Fe(211)$ surface.

the dominant pathway for methanation is the direct CO dissociation path. It has been suggested that there are two important properties of the transition metal catalyst determining the activity of methanation via a direct CO dissociation path: the barrier for CO dissociation and the binding strength of the main intermediates on the surface.[53,54] The low TOF of Fe is due to its too strong binding of the surface intermediates, especially O, as shown in Table S6 in the Supporting Information, although the CO dissociation barrier on the Fe(211) surface is the lowest among all the studied catalyst surfaces, as shown in Figure 6a. For Ni and Ni−Fe alloy catalyst, the dominant pathway is the CO → COH → C path, which agrees with previous studies of CO methanation over Ni-based catalyst[6,58,59] and the reaction rate is greatly limited by these two reactions. According to the calculations, CO hydrogenation to COH prefers to happen at a pure Ni step site, as shown in Figure 6b, while for COH to C dissociation it happens at a step site with one close by Fe atom bonding to the OH, as shown in Figure 6c. It demonstrates that Ni is primarily active toward CO hydrogenation because of its stronger binding to CO over Fe while Fe is more active in C−OH bond cleavage due to its strong binding to OH, as shown in Table S6 in the Supporting Information. This is proved by the calculated reaction barrier for COH formation and dissociation reactions, as shown in Figure 6a, which shows that the barrier for CO hydrogenation to COH is increased with increasing Fe concentration while the COH dissociation barrier on the contrary decreases. Most importantly, it explains why an optimal activity/TOF is found on the 4-Fe $Ni_3Fe(211)$ surface system since the Ni(211) surface bears the lack of Fe on the surface to stabilize the OH for COH dissociation while the 12-Fe NiFe(211) surface suffers from the absence of an active pure Ni step sites for CO hydrogenation to COH, as shown in Figure S5 in the Supporting Information.

Catalyst Design: How to Make the Most out of a Ni_3Fe alloy Catalyst? From the reaction kinetics analysis, we understand that the high activity of the 4-Fe $Ni_3Fe(211)$ catalyst system originates from its unique stable surface structure that consists of active sites for both CO activation (CO → COH) and CO dissociation (COH → C). It seems that if the catalyst can retain a surface structure that consists of the two active sites, it will be very active toward CO methanation, and the 4-Fe surface composition may not be a necessity. To verify this hypothesis, the reaction barriers of CO hydrogenation and COH dissociation on more $Ni_3Fe(211)$ surfaces that have the required surface sites are calculated. In total, there are 8 such surfaces which consist of 1 to 8 Fe atoms on the surface, respectively, as shown in Figure S4 in the Supporting Information, and the calculated reaction barriers are shown in Figure 7. The results indicate that the COH

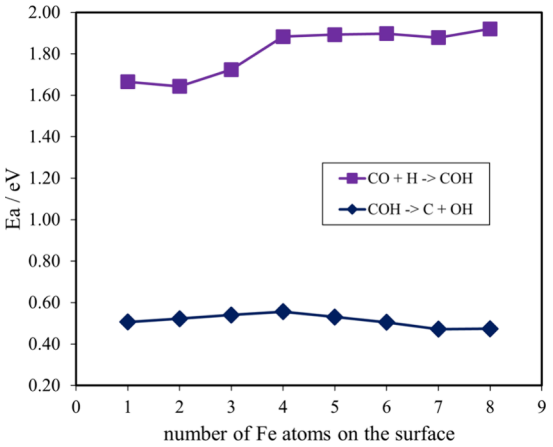

Figure 7. Reaction barriers for CO → COH and COH → C on different $Ni_3Fe(211)$ surfaces with various numbers (from 1 to 8) of surface Fe atoms.

dissociation barrier changes little with the change of surface Fe atoms, demonstrating the vital role of Fe in COH dissociation. For the CO hydrogenation reaction, the reaction barrier increases with an increase of surface Fe atoms, while a negligible effect on the reaction barriers is found when the number of surface Fe atoms reaches 4. This can be explained by the surface atoms stacking pattern of $Ni_3Fe(211)$, as shown in Figure S2. For surfaces that consist of Fe atoms less than 4, the Fe atoms will stay at a position close to the active step Ni site, while for surfaces having more Fe atoms, the Fe atom is located far from the active Ni site, which therefore cannot significantly affect the CO hydrogenation reaction. Most importantly, what Figure 7 indicates is that for surfaces with fewer surface Fe atoms, especially the 1-Fe surface, the reaction barrier of CO hydrogenation and COH dissociation is about 0.2 and 0.08 eV smaller than the 4Fe surface system, respectively, indicating a probable higher activity of the surface. The problem is, however, that these surfaces are not stable under reaction conditions according to the surface stability study, although a higher activity could be obtained from them. It proves that the 4-Fe surface atom pattern is not a

https://doi.org/10.1021/acscatal.4c02449
ACS Catal. 2024, 14, 11657−11665

necessity to obtain high CO methanation activity for the Ni_3Fe alloy catalyst but the stability of the active step sites for CO hydrogenation and dissociation under reaction conditions is on the contrary the most important activity-determining factor. Therefore, an optimal $Ni_3Fe(211)$ catalyst system should have a Ni-rich surface with a maximum pure Ni step site and sufficient Fe atoms close by to get the most (maximal activity) out of the catalyst for CO methanation. Especially, making catalysts with stable surfaces like the 1-Fe $Ni_3Fe(211)$ through support interaction and single metal alloy technique so that maximum active metal sites can be obtained would increase the catalyst activity furthermore.[55]

SUMMARY

In this study, we have devised a framework aimed at addressing the inverse design problem concerning the methanation of CO over Ni−Fe bimetallic alloy catalysts, and the goal is to determine a Ni−Fe composition and structure conducive to the desired active surface site motif during the catalytic process. Initially, we investigated the stability of various NiFe(211) and $Ni_3Fe(211)$ surfaces, encompassing all possible surface compositions (surface Ni/Fe atom ratio ranging from 0 to 1), under reaction conditions at different CO coverages since CO is found to be the primary surface species. Our findings indicate that the 4-Fe $Ni_3Fe(211)$ and 12-Fe NiFe(211) surfaces exhibit the highest stability across all conditions, indicating that the CO adsorption is not able to induce surface segregation. Subsequently, we developed a surface- and coverage-consistent microkinetic model (MKM) to determine the methanation turnover frequency (TOF) for various surfaces with distinct bulk and surface compositions that remain stable under reaction conditions. We established a correlation between the surface and bulk composition and reaction TOFs, with the 4-Fe $Ni_3Fe(211)$ surface site demonstrating the highest TOF.

To elucidate the underlying factors contributing to the high activity of the 4-Fe $Ni_3Fe(211)$ surface, we conducted reaction barrier calculations for the CO activation/dissociation steps, identified as the rate-controlling steps in CO methanation. Our analysis attributes the enhanced activity of the 4-Fe Ni_3Fe-(211) surface to a pure step Ni site facilitating hydrogenation of CO to COH, in conjunction with a neighboring Fe site promoting COH dissociation. To further validate our hypothesis, we calculated the reaction barriers for CO → COH and COH → C on various $Ni_3Fe(211)$ surfaces, which have active sites similar to those of the 4-Fe surface but exhibit lower stability under reaction conditions. Our results indicate that surfaces featuring a pure Ni step site and a nearby Fe site exhibit similar reaction barriers for the two rate-controlling steps. Notably, the 1-Fe $Ni_3Fe(211)$ surface displayed the lowest barriers, suggesting the potential for further activity enhancement despite its lower stability. This underscores the significance of the active site motif and its stability under reaction conditions in catalytic activity, rather than the presence of 4-Fe surface sites. Consequently, we propose that optimizing $Ni_{1-x}Fe_x$ catalysts for CO methanation may involve synthesizing Ni_3Fe catalysts with a focus on stabilizing the active site motif identified under reaction conditions. This could be achieved through advanced single-atom alloying to form a stable 1-Fe $Ni_3Fe(211)$ surface under the reaction conditions using optimized synthesis methods and supporting materials,[72] even though it is known to be thermodynamically unstable.

It is noteworthy that CO adsorption is found to be not able to induce surface metal atom segregation in our study due to a similar binding strength of CO on Ni and Fe. Despite being unable to test the surface-consistent MKM and unfortunately not showing the full inverse design solution process for the studied Ni−Fe alloy, our proposed framework still provides researchers with a protocol to address the catalyst inverse design problem, aiming to maximize activity, for other extensively studied reaction systems. Given that the proposed approach is purely theoretical and based on DFT calculations, combining experimental data with DFT-based MKM simulations can provide a more comprehensive understanding and enhance the accuracy of the design process. Experimental turnover frequency (TOF) data offer real-world validation and insights into catalytic performance under various conditions, while MKM simulations provide detailed mechanistic insights and active site information. By leveraging both approaches, the design process can be optimized, ensuring that the proposed active sites are not only theoretically efficient but also practically viable based on empirical evidence. However, this integration is beyond the scope of the current work, as we propose a theoretical protocol for the inverse design of catalysts, which will be explored in future studies.

ASSOCIATED CONTENT

Supporting Information

The Supporting Information is available free of charge at https://pubs.acs.org/doi/10.1021/acscatal.4c02449.

Details of the surface atom exchanging process, the top view of optimized clean Ni−Fe surface slab, description of the surface system stability calculations, adsorption site on the Ni−Fe alloy surface for CO binding and the optimized surface with various CO coverages, CO methanation reaction network and equations used to calculated the universal referenced binding energies for the surface intermediates, the binding free energies of reaction intermediates at 523 K on various Ni−Fe surfaces at different CO coverages, and the final converged MKM results from the self-consistent model (PDF)

AUTHOR INFORMATION

Corresponding Author

Jens K. Nørskov − *Catalysis Theory Center, Department of Physics, Technical University of Denmark, 2800 Kongens Lyngby, Denmark*; Email: jkno@dtu.dk

Authors

Wenqiang Yang − *Catalysis Theory Center, Department of Physics, Technical University of Denmark, 2800 Kongens Lyngby, Denmark; Department of Chemical Engineering, University of South Carolina, Columbia, South Carolina 29208, United States*; orcid.org/0000-0002-5839-4159

Zhenbin Wang − *Department of Materials Science and Engineering, City University of Hong Kong, Kowloon 999077, Hong Kong*; orcid.org/0000-0002-7016-9245

Complete contact information is available at: https://pubs.acs.org/10.1021/acscatal.4c02449

Notes

The authors declare no competing financial interest.

https://doi.org/10.1021/acscatal.4c02449
ACS Catal. 2024, 14, 11657−11665

■ ACKNOWLEDGMENTS

This project has received funding from Villum Fonden V-SUSTAIN (project name: 10-Fonde-1025-V-SUSTAIN; project number: 20886). Computational resources have been provided by Niflheim HPC Clusters at the Department of Physics of the Technical University of Denmark. The authors also gratefully acknowledge the computational and data resources provided by the Sophia HPC Cluster at the Technical University of Denmark.

■ REFERENCES

(1) d'Avezac, M.; Zunger, A. Finding the atomic configuration with a required physical property in multi-atom structures. *J. Phys.: Condens. Matter* **2007**, *19* (40), 402201.
(2) Piquini, P.; Graf, P. A.; Zunger, A. Band-gap design of quaternary (In,Ga)(As,Sb) semiconductors via the inverse-band-structure approach. *Phys. Rev. Lett.* **2008**, *100* (18), 186403.
(3) Kim, K.; Graf, P. A.; Jones, W. B. A genetic algorithm based inverse band structure method for semiconductor alloys. *J. Comput. Phys.* **2005**, *208* (2), 735−760.
(4) Franceschetti, A.; Zunger, A. The inverse band-structure problem of finding an atomic configuration with given electronic properties. *Nature* **1999**, *402* (6757), 60−63.
(5) Andersen, M.; Plaisance, C. P.; Reuter, K. Assessment of mean-field microkinetic models for CO methanation on stepped metal surfaces using accelerated kinetic Monte Carlo. *J. Chem. Phys.* **2017**, *147* (15), 152705.
(6) Andersson, M. P.; Abild-Pedersen, F.; Remediakis, I. N.; Bligaard, T.; Jones, G.; Engbæk, J.; Lytken, O.; Horch, S.; Nielsen, J. H.; Sehested, J.; Rostrup-Nielsen, J. R.; Nørskov, J. K.; Chorkendorff, I. Structure sensitivity of the methanation reaction: H2-induced CO dissociation on nickel surfaces. *J. Catal.* **2008**, *255* (1), 6−19.
(7) Dahl, S.; Logadottir, A.; Jacobsen, C. J. H.; Nørskov, J. K. Electronic factors in catalysis: the volcano curve and the effect of promotion in catalytic ammonia synthesis. *Applied Catalysis A: General* **2001**, *222* (1−2), 19−29.
(8) Dasgupta, A.; He, H.; Gong, R.; Shang, S. L.; Zimmerer, E. K.; Meyer, R. J.; Liu, Z. K.; Janik, M. J.; Rioux, R. M. Atomic control of active-site ensembles in ordered alloys to enhance hydrogenation selectivity. *Nat. Chem.* **2022**, *14* (5), 523−529.
(9) Ferrin, P.; Simonetti, D.; Kandoi, S.; Kunkes, E.; Dumesic, J. A.; Norskov, J. K.; Mavrikakis, M. Modeling ethanol decomposition on transition metals: a combined application of scaling and Bronsted-Evans-Polanyi relations. *J. Am. Chem. Soc.* **2009**, *131* (16), 5809−15.
(10) Gao, X.; Wang, Z.; Huang, Q.; Jiang, M.; Askari, S.; Dewangan, N.; Kawi, S. State-of-art modifications of heterogeneous catalysts for CO2 methanation - Active sites, surface basicity and oxygen defects. *Catal. Today* **2022**, *402*, 88−103.
(11) Greeley, J.; Nørskov, J. K. Combinatorial Density Functional Theory-Based Screening of Surface Alloys for the Oxygen Reduction Reaction. *J. Phys. Chem. C* **2009**, *113* (12), 4932−4939.
(12) Honkala, K.; Hellman, A.; Remediakis, I. N.; Logadottir, A.; Carlsson, A.; Dahl, S.; Christensen, C. H.; Norskov, J. K. Ammonia synthesis from first-principles calculations. *Science* **2005**, *307* (5709), 555−8.
(13) Jacobsen, C. J.; Dahl, S.; Clausen, B. S.; Bahn, S.; Logadottir, A.; Norskov, J. K. Catalyst design by interpolation in the periodic table: bimetallic ammonia synthesis catalysts. *J. Am. Chem. Soc.* **2001**, *123* (34), 8404−5.
(14) Jones, G.; Jakobsen, J.; Shim, S.; Kleis, J.; Andersson, M.; Rossmeisl, J.; Abildpedersen, F.; Bligaard, T.; Helveg, S.; Hinnemann, B. First principles calculations and experimental insight into methane steam reforming over transition metal catalysts. *J. Catal.* **2008**, *259* (1), 147−160.
(15) Kojima, R.; Aika, K.-i. Cobalt molybdenum bimetallic nitride catalysts for ammonia synthesis. *Applied Catalysis A: General* **2001**, *218* (1−2), 121−128.
(16) Liu, B.; Greeley, J. A density functional theory analysis of trends in glycerol decomposition on close-packed transition metal surfaces. *Phys. Chem. Chem. Phys.* **2013**, *15* (17), 6475−85.
(17) Loffreda, D.; Delbecq, F.; Vigne, F.; Sautet, P. Fast prediction of selectivity in heterogeneous catalysis from extended Bronsted-Evans-Polanyi relations: a theoretical insight. *Angew. Chem., Int. Ed. Engl.* **2009**, *48* (47), 8978−80.
(18) Salciccioli, M.; Vlachos, D. G. Kinetic Modeling of Pt Catalyzed and Computation-Driven Catalyst Discovery for Ethylene Glycol Decomposition. *ACS Catal.* **2011**, *1* (10), 1246−1256.
(19) Schumann, J.; Medford, A. J.; Yoo, J. S.; Zhao, Z.-J.; Bothra, P.; Cao, A.; Studt, F.; Abild-Pedersen, F.; Nørskov, J. K. Selectivity of Synthesis Gas Conversion to C2+ Oxygenates on fcc(111) Transition-Metal Surfaces. *ACS Catal.* **2018**, *8* (4), 3447−3453.
(20) Shetty, S.; Jansen, A. P.; van Santen, R. A. Direct versus hydrogen-assisted CO dissociation. *J. Am. Chem. Soc.* **2009**, *131* (36), 12874−5.
(21) Spencer, N. Iron single crystals as ammonia synthesis catalysts: Effect of surface structure on catalyst activity. *J. Catal.* **1982**, *74* (1), 129−135.
(22) Sutton, J. E.; Vlachos, D. G. Ethanol Activation on Closed-Packed Surfaces. *Ind. Eng. Chem. Res.* **2015**, *54* (16), 4213−4225.
(23) Theofanidis, S. A.; Galvita, V. V.; Sabbe, M.; Poelman, H.; Detavernier, C.; Marin, G. B. Controlling the stability of a Fe-Ni reforming catalyst: Structural organization of the active components. *Applied Catalysis B: Environmental* **2017**, *209*, 405−416.
(24) Van Santen, R. A. Complementary structure sensitive and insensitive catalytic relationships. *Acc. Chem. Res.* **2009**, *42* (1), 57−66.
(25) Wang, H. F.; Liu, Z. P. Comprehensive mechanism and structure-sensitivity of ethanol oxidation on platinum: new transition-state searching method for resolving the complex reaction network. *J. Am. Chem. Soc.* **2008**, *130* (33), 10996−1004.
(26) Yaccato, K.; Carhart, R.; Hagemeyer, A.; Lesik, A.; Strasser, P.; Volpe, A. F.; Turner, H.; Weinberg, H.; Grasselli, R. K.; Brooks, C. Competitive CO and CO2 methanation over supported noble metal catalysts in high throughput scanning mass spectrometer. *Applied Catalysis A: General* **2005**, *296* (1), 30−48.
(27) Yang, Q.; Kondratenko, V. A.; Petrov, S. A.; Doronkin, D. E.; Saraci, E.; Lund, H.; Arinchtein, A.; Kraehnert, R.; Skrypnik, A. S.; Matvienko, A. A.; Kondratenko, E. V. Identifying Performance Descriptors in CO(2) Hydrogenation over Iron-Based Catalysts Promoted with Alkali Metals. *Angew. Chem., Int. Ed. Engl.* **2022**, *61* (22), No. e202116517.
(28) Walker, E. A.; Mitchell, D.; Terejanu, G. A.; Heyden, A. Identifying Active Sites of the Water-Gas Shift Reaction over Titania Supported Platinum Catalysts under Uncertainty. *ACS Catal.* **2018**, *8* (5), 3990−3998.
(29) Simons, J. F. M.; de Heer, T. J.; van de Poll, R. C. J.; Muravev, V.; Kosinov, N.; Hensen, E. J. M. Structure Sensitivity of CO(2) Hydrogenation on Ni Revisited. *J. Am. Chem. Soc.* **2023**, *145* (37), 20289−20301.
(30) Wang, T.; Xi, Y.; Li, F. Alkyl C-O bond cleavage assisted by partial C-H activation on atomically dispersed catalysts and metal surfaces. *Chem. Catalysis* **2024**, *4* (2), 100892.
(31) Ding, K.; Gulec, A.; Johnson, A. M.; Schweitzer, N. M.; Stucky, G. D.; Marks, L. D.; Stair, P. C. Identification of active sites in CO oxidation and water-gas shift over supported Pt catalysts. *Science* **2015**, *350* (6257), 189−92.
(32) Nørskov, J. K.; Rossmeisl, J.; Logadottir, A.; Lindqvist, L.; Kitchin, J. R.; Bligaard, T.; Jónsson, H. Origin of the Overpotential for Oxygen Reduction at a Fuel-Cell Cathode. *J. Phys. Chem. B* **2004**, *108* (46), 17886−17892.
(33) Jaramillo, T. F.; Jorgensen, K. P.; Bonde, J.; Nielsen, J. H.; Horch, S.; Chorkendorff, I. Identification of active edge sites for electrochemical H2 evolution from MoS2 nanocatalysts. *Science* **2007**, *317* (5834), 100−2.
(34) Skúlason, E.; Tripkovic, V.; Björketun, M. E.; Gudmundsdóttir, S.; Karlberg, G.; Rossmeisl, J.; Bligaard, T.; Jónsson, H.; Nørskov, J. K.

https://doi.org/10.1021/acscatal.4c02449
ACS Catal. 2024, 14, 11657−11665

Modeling the Electrochemical Hydrogen Oxidation and Evolution Reactions on the Basis of Density Functional Theory Calculations. *J. Phys. Chem. C* **2010**, *114* (42), 18182−18197.
(35) Hansen, H. A.; Viswanathan, V.; Nørskov, J. K. Unifying Kinetic and Thermodynamic Analysis of 2 e- and 4 e- Reduction of Oxygen on Metal Surfaces. *J. Phys. Chem. C* **2014**, *118* (13), 6706−6718.
(36) Seh, Z. W.; Kibsgaard, J.; Dickens, C. F.; Chorkendorff, I.; Norskov, J. K.; Jaramillo, T. F. Combining theory and experiment in electrocatalysis: Insights into materials design. *Science* **2017**, *355* (6321), aad4998.
(37) Verdaguer-Casadevall, A.; Deiana, D.; Karamad, M.; Siahrostami, S.; Malacrida, P.; Hansen, T. W.; Rossmeisl, J.; Chorkendorff, I.; Stephens, I. E. Trends in the electrochemical synthesis of H2O2: enhancing activity and selectivity by electrocatalytic site engineering. *Nano Lett.* **2014**, *14* (3), 1603−8.
(38) Viswanathan, V.; Hansen, H. A.; Rossmeisl, J.; Nørskov, J. K. Universality in Oxygen Reduction Electrocatalysis on Metal Surfaces. *ACS Catal.* **2012**, *2* (8), 1654−1660.
(39) Nematollahi, B.; Rezaei, M.; Lay, E. N. Selective methanation of carbon monoxide in hydrogen rich stream over Ni/CeO2 nanocatalysts. *Journal of Rare Earths* **2015**, *33* (6), 619−628.
(40) Gao, Z.; Dai, Q.; Ma, H.; Li, Z. Ceria supported nickel catalysts for CO removal from H2-rich gas. *Journal of Rare Earths* **2016**, *34* (12), 1213−1220.
(41) Yu, Y.; Jin, G.; Wang, Y.; Guo, X. Synthesis of natural gas from CO methanation over SiC supported Ni-Co bimetallic catalysts. *Catal. Commun.* **2013**, *31*, 5−10.
(42) Kambolis, A.; Schildhauer, T. J.; Krocher, O. CO Methanation for Synthetic Natural Gas Production. *Chimia (Aarau)* **2015**, *69* (10), 608−13.
(43) Garbis, P.; Jess, A. Selective CO Methanation in H2-Rich Gas for Household Fuel Cell Applications. *Energies* **2020**, *13* (11), 2844.
(44) Trimm, D. L.; Önsan, Z. I. Onboard Fuel Conversion for Hydrogen-Fuel-Cell-Driven Vehicles. *Catalysis Reviews* **2001**, *43* (1−2), 31−84.
(45) Panagiotopoulou, P.; Kondarides, D. I.; Verykios, X. E. Selective methanation of CO over supported noble metal catalysts: Effects of the nature of the metallic phase on catalytic performance. *Applied Catalysis A: General* **2008**, *344* (1−2), 45−54.
(46) Tada, S.; Kikuchi, R.; Takagaki, A.; Sugawara, T.; Oyama, S. T.; Urasaki, K.; Satokawa, S. Study of Ru Ni/TiO2 catalysts for selective CO methanation. *Applied Catalysis B: Environmental* **2013**, *140−141*, 258−264.
(47) Tada, S.; Minori, D.; Otsuka, F.; Kikuchi, R.; Osada, K.; Akiyama, K.; Satokawa, S. Effect of Ru and Ni ratio on selective CO methanation over Ru-Ni/TiO2. *Fuel* **2014**, *129*, 219−224.
(48) Shimoda, N.; Fujiwara, M.; Tani, K.; Shoji, D.; Takahashi, M.; Akiyama, K.; Satokawa, S. Durability of Ni/TiO2 catalyst containing trace chlorine for CO selective methanation. *Applied Catalysis A: General* **2018**, *557*, 7−14.
(49) Martínez T, L. M.; Muñoz, A.; Pérez, A.; Laguna, O. H.; Bobadilla, L. F.; Centeno, M. A.; Odriozola, J. A. The effect of support surface hydroxyls on selective CO methanation with Ru based catalysts. *Applied Catalysis A: General* **2022**, *641*, 118678.
(50) Hatta, A. H.; Jalil, A. A.; Hassan, N. S.; Hamid, M. Y. S.; Rahman, A. F. A.; Aziz, M. A. H. A short review on Ni-based catalyst supporter for carbon monoxide (CO) methanation process. *Journal of Physics: Conference Series* **2022**, *2259* (1), 012025.
(51) Wang, W.; Toshcheva, E.; Ramirez, A.; Shterk, G.; Ahmad, R.; Caglayan, M.; Cerrillo, J. L.; Dokania, A.; Clancy, G.; Shoinkhorova, T. B.; Hijazi, N.; Cavallo, L.; Gascon, J. Bimetallic Fe-Co catalysts for the one step selective hydrogenation of CO2 to liquid hydrocarbons. *Catalysis Science & Technology* **2023**, *13* (5), 1527−1540.
(52) Hwang, S.; Lee, J.; Hong, U. G.; Jung, J. C.; Koh, D. J.; Lim, H.; Byun, C.; Song, I. K. Hydrogenation of carbon monoxide to methane over mesoporous nickel-M-alumina (M = Fe, Ni, Co, Ce, and La) xerogel catalysts. *Journal of Industrial and Engineering Chemistry* **2012**, *18* (1), 243−248.
(53) Andersson, M.; Bligaard, T.; Kustov, A.; Larsen, K.; Greeley, J.; Johannessen, T.; Christensen, C.; Norskov, J. Toward computational screening in heterogeneous catalysis: Pareto-optimal methanation catalysts. *J. Catal.* **2006**, *239* (2), 501−506.
(54) Kustov, A. L.; Frey, A. M.; Larsen, K. E.; Johannessen, T.; Nørskov, J. K.; Christensen, C. H. CO methanation over supported bimetallic Ni-Fe catalysts: From computational studies towards catalyst optimization. *Applied Catalysis A: General* **2007**, *320*, 98−104.
(55) Pandey, D.; Deo, G. Promotional effects in alumina and silica supported bimetallic Ni-Fe catalysts during CO2 hydrogenation. *J. Mol. Catal. A: Chem.* **2014**, *382*, 23−30.
(56) Sehested, J.; Larsen, K. E.; Kustov, A. L.; Frey, A. M.; Johannessen, T.; Bligaard, T.; Andersson, M. P.; Nørskov, J. K.; Christensen, C. H. Discovery of technical methanation catalysts based on computational screening. *Top. Catal.* **2007**, *45* (1−4), 9−13.
(57) Kang, S.-H.; Ryu, J.-H.; Kim, J.-H.; Seo, S.-J.; Yoo, Y.-D.; Sai Prasad, P. S.; Lim, H.-J.; Byun, C.-D. Co-methanation of CO and CO2 on the Ni X -Fe1-X /Al2O3 catalysts; effect of Fe contents. *Korean Journal of Chemical Engineering* **2011**, *28* (12), 2282−2286.
(58) Wind, T. L.; Falsig, H.; Sehested, J.; Moses, P. G.; Nguyen, T. T. M. Comparison of mechanistic understanding and experiments for CO methanation over nickel. *J. Catal.* **2016**, *342*, 105−116.
(59) Lausche, A. C.; Medford, A. J.; Khan, T. S.; Xu, Y.; Bligaard, T.; Abild-Pedersen, F.; Nørskov, J. K.; Studt, F. On the effect of coverage-dependent adsorbate-adsorbate interactions for CO methanation on transition metal surfaces. *J. Catal.* **2013**, *307*, 275−282.
(60) Blochl, P. E. Projector augmented-wave method. *Phys. Rev. B Condens Matter* **1994**, *50* (24), 17953−17979.
(61) Kresse, G.; Furthmuller, J. Efficient iterative schemes for ab initio total-energy calculations using a plane wave basis set. *Phys. Rev. B Condens Matter* **1996**, *54* (16), 11169−11186.
(62) Perdew, J. P.; Burke, K.; Ernzerhof, M. Generalized Gradient Approximation Made Simple [Phys. Rev. Lett. 77, 3865 (1996)]. *Phys. Rev. Lett.* **1997**, *78* (7), 1396−1396.
(63) Kresse, G.; Joubert, D. From ultrasoft pseudopotentials to the projector augmented-wave method. *Phys. Rev. B* **1999**, *59* (3), 1758−1775.
(64) Perdew, J. P.; Yue, W. Accurate and simple density functional for the electronic exchange energy: Generalized gradient approximation. *Phys. Rev. B Condens Matter* **1986**, *33* (12), 8800−8802.
(65) Hammer, B.; Hansen, L. B.; Nørskov, J. K. Improved adsorption energetics within density-functional theory using revised Perdew-Burke-Ernzerhof functionals. *Phys. Rev. B* **1999**, *59* (11), 7413−7421.
(66) Kaplan, A. D.; Perdew, J. P. Laplacian-level meta-generalized gradient approximation for solid and liquid metals. *Physical Review Materials* **2022**, *6* (8), 083803.
(67) Monkhorst, H. J.; Pack, J. D. Special points for Brillouin-zone integrations. *Phys. Rev. B* **1976**, *13* (12), 5188−5192.
(68) Henkelman, G.; Uberuaga, B. P.; Jónsson, H. A climbing image nudged elastic band method for finding saddle points and minimum energy paths. *J. Chem. Phys.* **2000**, *113* (22), 9901−9904.
(69) Heyden, A.; Bell, A. T.; Keil, F. J. Efficient methods for finding transition states in chemical reactions: comparison of improved dimer method and partitioned rational function optimization method. *J. Chem. Phys.* **2005**, *123* (22), 224101.
(70) Henkelman, G.; Jónsson, H. A dimer method for finding saddle points on high dimensional potential surfaces using only first derivatives. *J. Chem. Phys.* **1999**, *111* (15), 7010−7022.
(71) Guo, C.; Mao, Y.; Yao, Z.; Chen, J.; Hu, P. Examination of the key issues in microkinetics: CO oxidation on Rh(**1 1 1**). *J. Catal.* **2019**, *379*, 52−59.
(72) Li, W.; Guo, Z.; Yang, J.; Li, Y.; Sun, X.; He, H.; Li, S.; Zhang, J. Advanced Strategies for Stabilizing Single-Atom Catalysts for Energy Storage and Conversion. *Electrochemical Energy Reviews* **2022**, *5* (3), 9.

https://doi.org/10.1021/acscatal.4c02449
ACS Catal. 2024, 14, 11657−11665